

Neutralino and Chargino Production in $U(1)'$ at the LHC

Mariana Frank^a, Levent Selbuz^{a,b}, and Ismail Turan^c

^a*Department of Physics, Concordia University,*

7141 Sherbrooke St. West, Montreal, Quebec, Canada H4B 1R6,

^b*Department of Engineering Physics,*

Ankara University, TR06100 Ankara, Turkey, and

^c*Department of Physics, Middle East Technical University, Ankara TR06800, Turkey*

Abstract

We examine the production and the decay modes of neutralinos and charginos in a softly-broken supersymmetric model with an extra Abelian symmetry $U(1)'$. We perform the study in a $U(1)'$ model with a secluded sector, where the tension between the electroweak scale and developing a large enough mass for Z' is resolved by incorporating three additional $SU(2)$ singlet fields into the model. Although the chargino sector is the same as in the MSSM, the neutralino sector of the model is very rich: five new fermion fields are added to the neutral sector bring the total neutralino states to nine. We implement the model into standard packages and perform a detailed and systematic analysis of production and decay modes at the LHC, for three different scenarios, and concentrating on final signals (1) $1\ell + jets + \cancel{E}_T$, (2) $2\ell + jets + \cancel{E}_T$ and (3) $3\ell + 0jets + \cancel{E}_T$, and comment on the case with $0\ell + jets + \cancel{E}_T$. We discuss backgrounds and indicate how these signals can be observed, and how the model can be distinguished from other supersymmetric model scenarios.

PACS numbers: 12.60.Cn, 12.60.Jv, 14.80.Ly.

Keywords: Supersymmetry, Neutralino, Chargino, LSP, LHC.

I. INTRODUCTION AND MOTIVATION

After the recent discovery of the new resonance most likely to be the Higgs boson at ATLAS [1] and CMS [2], the top priority for LHC shifts to the search for physics effects beyond the SM. Supersymmetry is the leading candidate of physics beyond the SM. The Minimal Supersymmetric Standard Model (MSSM), motivated by the resolution of such long standing problems of the SM as the gauge hierarchy problem, the existence of dark matter, and the gauge unification, is arguably the most popular ‘new physics’ scenario, the perturbative extension of the SM beyond electroweak scales. However, recent LHC results [3] rule out some of the parameter regions of the constrained version of MSSM (CMSSM), and point towards a heavy spectrum of supersymmetric partners, if this particular version of SUSY is realized in nature.

Extensions of the MSSM gauge symmetry by additional $U(1)'$ Abelian groups are some of the best motivated extensions of the standard model (SM). The justification is not so much based on resolving some of problems in MSSM, but by the fact that such an extension is minimal, and it is well motivated in superstring theories [4], grand unified theories [5] and in dynamically broken electroweak theories [6]. The additional gauge group introduces one extra neutral gauge boson Z' . The simplest version of $U(1)'$ extended supersymmetric models involve also an additional singlet S , charged under $U(1)'$, whose vacuum expectation value (VEV) is responsible for the breaking of $U(1)'$. This VEV simultaneously generates dynamically an effective μ term, an elegant resolution of the so-called μ problem [7], and is responsible for the mass of the Z' boson. Some versions of these extended symmetries also allow right-handed neutrinos into the spectrum. Small neutrino masses consistent with neutrino oscillation phenomenology are usually explained by the see-saw mechanism [8]. In the Type II see-saw mechanism, large Majorana masses for right-handed neutrinos are responsible for inducing small Majorana masses for left-handed neutrinos. The choice of $U(1)'$ symmetry would determine the magnitude and type of neutrino masses [9]. For the purpose of this investigation, we assume a $U(1)'$ extended form of the MSSM that contains Dirac-type neutrino masses as in [10], although viable models exist for Majorana masses as well [11]. This model shares some of the advantages of the next-to-minimal supersymmetric standard models (NMSSM). In the MSSM at tree-level, the Higgs mass is bound by $m_h \leq M_{Z'}$. To alleviate this problem, large stop masses and large trilinear A_t -terms are

added to the MSSM [12]. In $U(1)'$, the addition of one singlet field provides new tree-level contributions to the F -term, which stabilize the Higgs mass naturally at a larger value [13], thus accommodating a lightest Higgs boson mass at 125 GeV.

In the minimal version of extended $U(1)'$ symmetry models, loops generate a mixing term for $Z - Z'$ bosons, which in turn is constrained by the electroweak precision data to be $\mathcal{O}(10^{-3})$, or smaller, while collider constraints on Z' mass require it to be heavy. In the minimal $U(1)'$ model, explored in Ref. [14], it is shown that the difficulty to induce a small μ_{eff} while satisfying the Z' mass bound, which is around 1 TeV, stems from the fact that both are proportional to the VEV of the additional scalar field S . The resolution is provided in a non-minimal version of the $U(1)'$ extended MSSM, in which several singlet (S_i) fields are introduced to resolve the conflict between maintaining the electroweak scale and developing a large enough mass for Z' . One needs three additional scalars to ameliorate the picture, and the VEVs of the new scalars to be kept large [15, 16]. A comparative study of LHC signals of sneutrino production and decays in the MSSM and in a supersymmetric model with a secluded $U(1)'$ breaking sector has been performed in [17]. We refer to this version of the model as secluded $U(1)'$, an abbreviated notation for the gauge symmetry underlying the model, $SU(3)_c \otimes SU(2)_L \otimes U(1)_Y \otimes U(1)'$, with a non-minimal $U(1)'$.

Direct or indirect detection of the superpartners of the Standard Model particles, considered the definitive signal for supersymmetry, is an important part of the experimental program of the LHC. One could consider two distinct phenomenological approaches to SUSY searches. One approach is based on the latest available experimental information. This method has the advantage of incorporating all the relevant experimental constraints, but the disadvantage of becoming quickly obsolete, as more data becomes available; also experimental data forecasts rarely impose direct and precise constraints, as many free parameters are involved. The other approach is to look into models for interesting benchmark scenarios, which illustrate model-specific possibilities. These benchmarks may incorporate some, but not all, present experimental constraints, and serve as indicators of possible experimental signatures. For instance, the cosmological relic density constraint for models where the lightest neutralino is the Lightest Supersymmetric Particle (LSP) is a definite constraint; so are consistency with low-energy phenomenology, such as flavor-changing and CP-violating processes. We follow the latter approach here.

The LHC has already devoted a great deal of time and effort to searches for supersymmet-

ric partners. Gluinos and scalar quarks are expected to be produced copiously at a hadron collider, though no signals are seen [19]. However, these states are expected to be heavy, and, except for the LSP in the R -parity conserving supersymmetry, the superpartners are expected to decay instantaneously into SM particles plus the LSP, detected as missing energy. Neutralinos and charginos, expected to be lighter, can play an important role as they occur in various steps in the cascade decays of certain supersymmetric particles (squarks, gluinos, etc.), and thus they would be abundantly produced at the LHC. Besides direct signals at the colliders, charginos and neutralinos can give indirect indications of their existence. Both can have implications on Higgs physics. For instance, it is possible that the Higgs invisible width could be due to decays into neutralinos, while the charginos could be responsible for the enhancement of the Higgs decays into $\gamma\gamma$ [20].

The production of neutralinos at hadron colliders is an important part of the program of SUSY searches. One special reason is related to the possibility that the lightest neutralino state ($\tilde{\chi}_1^0$) is in fact the LSP. Searches for charginos and neutralinos have not yielded any results so far. However, all searches come with conditions attached, due to the many alternative models, different sources of SUSY breaking, classes of compactification, and thus extensive possible parameter space; and most analyses focus on MSSM. We summarize the results of some of the recent searches. At ATLAS, chargino masses between 110 and 340 GeV are excluded in direct production of wino-like pairs, decaying into LSP via on-shell slepton, for a 10 GeV neutralino, at 95% C.L. For models with decays into intermediate degenerate sleptons, the lightest chargino $\tilde{\chi}_1^+$ and second lightest neutralino $\tilde{\chi}_2^0$ are ruled out up to masses of 500 GeV [21]. CMS analyzed final states with three leptons in conjunction with two *jets* to rule out chargino and neutralino masses between 200 and 500 GeV, for models where $\text{BR}(\tilde{\chi}^{0(-)} \rightarrow Z(W))$ leptons is large [22].

Despite all the negative searches, one might think that, even if no direct signals of supersymmetry have been observed, the presence of dark matter in the universe is already an indirect signal for supersymmetry. In most variants of the MSSM consistent with relic density calculations, the LSP is the lightest neutralino. Thus studies of possible supersymmetric particles at colliders are worthwhile pursuits.

The production of neutralinos is of special interest in the secluded sector $U(1)'$ model. The additional singlet fields introduced to generate the $Z - Z'$ mass splitting mass are difficult to detect, and expected to be heavy. However, their fermion partners, the neutralinos, could

be light and enhance the direct and cascade production at colliders. This would then be the best test of the secluded sector.

With this in mind, we perform a comprehensive study of LHC signals of neutralino (and chargino) production and decays in a supersymmetric model with a secluded $U(1)'$ breaking sector, concentrating on highlighting the contributions of the additional singlino-like neutralino states which appear in the SUSY cascade decays and alter the signatures of the secluded $U(1)'$ model as compared to the MSSM. We analyze the signals, classified according to the number of leptons in the final states, and we also include estimates of possible Standard Model backgrounds in three different scenarios. Unfortunately, no recent corresponding analysis is available for MSSM [23], making a direct comparison difficult. While in a previous work [24], we showed that in a minimal $U(1)'$ model (with one extra singlet boson), choosing the right-handed sneutrino as the LSP could be consistent with the excess positron observed in satellite experiments, for the purpose of this work, in the secluded sector $U(1)'$ we take the lightest neutralino consistently to be the lightest supersymmetric particle (LSP) and therefore a dark matter (DM) candidate.

The outline of this paper is as follows. We briefly introduce the model in Section II, with particular emphasis on the neutralino and chargino sector, then give the parameters and physical masses of supersymmetric particles in the $U(1)'$ model in Section III. For each benchmark point, we insure that DM candidate of the $U(1)'$ model yields relic densities consistent with the WMAP range of cold dark matter density [25]. We then perform a comprehensive analysis of the production, decays and detectability of neutralinos and chargino within these benchmark supersymmetric parameter points. During this analysis we focus on three types of detector signatures: (1) $1\ell + jets + \cancel{E}_T$, (2) $2\ell + jets + \cancel{E}_T$ and (3) $3\ell + 0jets + \cancel{E}_T$, and we present the results of our simulation analysis for the LHC. In Section IV we summarize and conclude the analysis. We leave the details of the composition of physical neutralinos in the model to the Appendix A, and list some characteristic decay patterns in the three scenarios in Appendix B.

II. THE SECLUDED $U(1)'$ MODEL

We summarize here the salient features of the secluded $U(1)'$ model, with particular emphasis on the chargino and neutralino sector.

The $U(1)'$ charge assignments which generate the term μ_{eff} , of the form $\lambda_s \frac{\langle S \rangle}{\sqrt{2}} H_u H_d$, induce mixed anomalies between the $U(1)'$ and the $SU(3)_C \times SU(2)_L \times U(1)_Y$ groups. The cancellation of these anomalies requires introduction of exotic fermions, vector-like with respect to the MSSM, but chiral under the $U(1)'$ group. These fields introduce new D -terms in the superpotential.

The superpotential of the model contains Yukawa couplings for quarks and leptons, and the couplings for the exotic fields and is given by

$$\begin{aligned} \widehat{W} = & h_u \widehat{Q} \cdot \widehat{H}_u \widehat{U} + h_d \widehat{Q} \cdot \widehat{H}_d \widehat{D} + h_e \widehat{L} \cdot \widehat{H}_d \widehat{E} + h_s \widehat{S} \widehat{H}_u \cdot \widehat{H}_d + \frac{1}{M_R} \widehat{S}_1 \widehat{L} \cdot \widehat{H}_u \mathbf{h}_\nu \widehat{N} + \bar{h}_s \widehat{S}_1 \widehat{S}_2 \widehat{S}_3 \\ & + \sum_{i=1}^{n_Q} h_Q^i \widehat{S} \widehat{Q}_i \widehat{\bar{Q}}_i + \sum_{j=1}^{n_L} h_L^j \widehat{S} \widehat{\mathcal{L}}_j \widehat{\bar{\mathcal{L}}}_j, \end{aligned} \quad (1)$$

where the fields \mathcal{Q} , \mathcal{L} are the exotic fermions, M_R is a large mass scale and h_ν is the Yukawa coupling responsible for generating neutrino masses. In addition, the Lagrangian contains soft-breaking terms for the secluded sector

$$\begin{aligned} V_{soft} = & (m_{SS_1}^2 S S_1 + m_{SS_2}^2 S S_2 + m_{S_1 S_2}^2 S_1^\dagger S_2 + h.c.) + m_{H_u}^2 |H_u|^2 + m_{H_d}^2 |H_d|^2 + m_S^2 |S|^2 \\ & + \sum_{i=1}^3 m_{S_i}^2 |S_i|^2 - (A_s h_s S H_u H_d + A_{\bar{s}} \bar{h}_s S_1 S_2 S_3 + h.c.). \end{aligned} \quad (2)$$

The symmetry-breaking sector of the model is very rich. There are a number of CP -even and CP -odd Higgs fields. Finding an acceptable minimum of the Higgs potential is not a trivial task, even at the tree level. We leave the details for a forthcoming publication [18].

The $U(1)'$ charges of the fields satisfy a number of conditions arising the requirement of cancellation of gauge and gravitational anomalies. For instance, the charges for Higgs fields in the model are chosen so that $Q'_S = -Q'_{S_1} = -Q'_{S_2} = \frac{1}{2}Q'_{S_3}$, $Q'_{H_u} + Q'_{H_d} + Q'_S = 0$. The $U(1)'$ charge of the quark doublet \widehat{Q} is kept as a free parameter after the normalization $Q'_{H_u} = -2$, $Q'_{H_d} = 1$, $Q'_S = 1$, $Q'_{S_1} = -1$, $Q'_{S_2} = -1$, $Q'_{S_3} = 2$. A more detailed analysis of the secluded sector $U(1)'$ model, including the complete list of conditions for anomalies cancellation in the model, the Lagrangian as well as the complete charge assignments of the SM and exotic quarks and leptons in the model can be found in [17]. We forgo the complete discussion here and concentrate ourselves on the chargino and neutralino sector.

A. Charginos and Neutralinos

In $U(1)'$ models chargino sector is unaltered. However, chargino mass eigenstates become dependent upon $U(1)'$ breaking scale through μ_{eff} parameter in their mass matrix:

$$M_{\chi^\pm} = \begin{pmatrix} M_2 & M_W \sqrt{2} \sin \beta \\ M_W \sqrt{2} \cos \beta & \mu_{eff} \end{pmatrix} \quad (3)$$

which can be diagonalized by biunitary transformation

$$U^* M_{\chi^\pm} V^{-1} = \text{Diag}(\tilde{M}_{\chi_1^\pm}, \tilde{M}_{\chi_2^\pm}), \quad (4)$$

where U and V are unitary mixing matrices.

More importantly for this study, the $U(1)'$ model has five additional fermion fields in the neutral sector: the $U(1)'$ gauge fermion \tilde{Z}' and four singlinos \tilde{S} , \tilde{S}_1 , \tilde{S}_2 , \tilde{S}_3 , in total, nine neutralino states $\tilde{\chi}_i^0$ ($i = 1, \dots, 9$) [15]:

$$\tilde{\chi}_i^0 = \sum_a \mathcal{N}_{ia}^0 \tilde{G}_a, \quad (5)$$

where the mixing matrix \mathcal{N}_{ia}^0 connects the gauge-basis neutral fermion states to the physical-basis neutralinos $\tilde{\chi}_i^0$. The neutralino masses $M_{\tilde{\chi}_i^0}$ are obtained through diagonalization $\mathcal{N}^0 \mathcal{M} \mathcal{N}^{0T} = \text{Diag} \{M_{\tilde{\chi}_1^0}, \dots, M_{\tilde{\chi}_9^0}\}$. The 9×9 neutral fermion mass matrix is

$$\mathcal{M} = \begin{pmatrix} M_{\tilde{Y}} & 0 & -M_{\tilde{Y}\tilde{H}_d} & M_{\tilde{Y}\tilde{H}_u} & 0 & M_{\tilde{Y}\tilde{Z}'} & 0 & 0 & 0 \\ 0 & M_{\tilde{W}} & M_{\tilde{W}\tilde{H}_d} & -M_{\tilde{W}\tilde{H}_u} & 0 & 0 & 0 & 0 & 0 \\ -M_{\tilde{Y}\tilde{H}_d} & M_{\tilde{W}\tilde{H}_d} & 0 & -\mu & -\mu_{H_u} & \mu'_{H_d} & 0 & 0 & 0 \\ M_{\tilde{Y}\tilde{H}_u} & -M_{\tilde{W}\tilde{H}_u} & -\mu & 0 & -\mu_{H_d} & \mu'_{H_u} & 0 & 0 & 0 \\ 0 & 0 & -\mu_{H_u} & -\mu_{H_d} & 0 & \mu'_S & 0 & 0 & 0 \\ M_{\tilde{Y}\tilde{Z}'} & 0 & \mu'_{H_d} & \mu'_{H_u} & \mu'_S & M_{\tilde{Z}'} & \mu'_{S_1} & \mu'_{S_2} & \mu'_{S_3} \\ 0 & 0 & 0 & 0 & 0 & \mu'_{S_1} & 0 & -\frac{\bar{h}_s v_{s3}}{\sqrt{2}} & -\frac{\bar{h}_s v_{s2}}{\sqrt{2}} \\ 0 & 0 & 0 & 0 & 0 & \mu'_{S_2} & -\frac{\bar{h}_s v_{s3}}{\sqrt{2}} & 0 & -\frac{\bar{h}_s v_{s1}}{\sqrt{2}} \\ 0 & 0 & 0 & 0 & 0 & \mu'_{S_3} & -\frac{\bar{h}_s v_{s2}}{\sqrt{2}} & -\frac{\bar{h}_s v_{s1}}{\sqrt{2}} & 0 \end{pmatrix}. \quad (6)$$

The gaugino masses and mixing mass parameter between the $U(1)_Y$ and $U(1)'$ gauginos are generated by the soft symmetry breaking terms.

$$M_{\tilde{Z}'} = \frac{M_{\tilde{Y}'}}{\cos^2 \chi} - 2 \frac{\tan \chi}{\cos \chi} M_{\tilde{Y}\tilde{Y}'} + M_{\tilde{Y}} \tan^2 \chi, \quad M_{\tilde{Y}\tilde{Z}'} = \frac{M_{\tilde{Y}\tilde{Y}'}}{\cos \chi} - M_{\tilde{Y}} \tan \chi, \quad (7)$$

with χ the angle describing kinetic mixing. The remaining entries in (6) are generated by the MSSM soft breaking masses in the Higgs sector. The mass mixing terms are

$$\begin{aligned} M_{\tilde{Y}\tilde{H}_d} &= M_Z \sin \theta_W \cos \beta, & M_{\tilde{Y}\tilde{H}_u} &= M_Z \sin \theta_W \sin \beta, \\ M_{\tilde{W}\tilde{H}_d} &= M_Z \cos \theta_W \cos \beta, & M_{\tilde{W}\tilde{H}_u} &= M_Z \cos \theta_W \sin \beta, \end{aligned} \quad (8)$$

and the effective μ couplings in each sector

$$\begin{aligned} \mu_{H_d} &= h_s \frac{v_d}{\sqrt{2}}, & \mu_{H_u} &= h_s \frac{v_u}{\sqrt{2}}, & \mu'_{H_d} &= g_{Y'} Q'_{H_d} v_d, \\ \mu'_{H_u} &= g_{Y'} Q'_{H_u} v_u, & \mu'_S &= g_{Y'} Q'_S v_s, & \mu'_{S_i} &= g_{Y'} Q'_{S_i} v_{s_i}, \end{aligned} \quad (9)$$

with $g_{Y'}$ the coupling constant of $U(1)'$. For the numerical analysis we choose the usual value at GUT scale $g_{Y'} = \sqrt{\frac{5}{3}} g \tan \theta_W$ and $\chi = 0$. The production and decay of neutralinos in the $U(1)'$ model without a secluded sector has been studied previously in [26].

III. CHARGINOS AND NEUTRALINOS IN $U(1)'$ AT THE LHC

A. $U(1)'$ Benchmark Points and Relic Density

Charginos and neutralinos, once produced, will decay following a pattern dictated by the benchmark parameters of the model. These scenarios would have definite predictions for the production and abundance of the lightest neutralino, assumed here to be the LSP. We proceed by evaluating the relic density of the lightest neutralino in the model, and subject it to the constraints from WMAP of cold dark matter.

For this task we specify three benchmark scenarios for the secluded $U(1)'$, denoted as Scenario A, Scenario B and Scenario C, by fixing the additional parameters to agree with phenomenological constraints on masses [27]. These benchmark points are given in Table I. For each benchmark scenario, the mass spectra obtained are given in Table II. As seen from Table I, the VEVs of the additional scalars (S_1, S_2 and S_3) $v_{s_i}, i = 1, 2, 3$ are mostly taken above the TeV scale so that the Z' mass bound is satisfied no matter what the VEV of the

scalar field S is chosen. In fact, for convenience, the parameters μ_{eff} and h_s are taken as free parameters and the VEV of S is determined accordingly using the relation

$$\mu_{eff} = \frac{h_s \langle S \rangle}{\sqrt{2}}. \quad (10)$$

From Table II it is seen that in Scenario A, both left and right scalar leptons are light and close in mass, thus allowing for two body decays of neutralinos into either mass-shell scalar leptons. We note that the lightest Higgs boson is at around 80 GeV, and not observed, while the second Higgs boson is within the ATLAS/CMS range. The Higgs sector parameters can be fine-tuned and do not affect the specific calculations in this paper. The lightest pseudoscalar boson decays invisibly and does not conflict with any present data. Scenario A has six light neutralinos (below 500 GeV) to highlight the spectrum and signal outcomes at the LHC. The fourth neutralino and lightest chargino are close in mass. In this scenario, dominant decays will be into neutralino pairs. In Scenario B, the right scalar leptons are heavy and the lightest chargino has approximately the same mass as the fifth neutralino. The lightest Higgs is in the ATLAS/CMS range. In this scenario, dominant decays will be into neutralino pairs. Scenario C has been designed to maximize the $3\ell + 0jets + \cancel{E}_T$ signal. The lightest chargino is mass degenerate with the NLSP, enhancing the decay into $3\ell + 0jets + \cancel{E}_T$.

The production cross sections for the scattering $pp \rightarrow \tilde{\chi}_i \tilde{\chi}_j$ processes are listed in Table III for three benchmark scenarios of the secluded $U(1)'$ model. The values were obtained implementing the secluded $U(1)'$ model into **CalcHEP** [28] with the help of **LanHEP** [29]. The parton distributions have been parametrized by using **CTEQ6M** of **LHAPDF** [30]. The total cross sections in Scenario A are of the order 1 pb for $pp \rightarrow \tilde{\chi}_4^0 \tilde{\chi}_1^\pm$ and large for, in order, $pp \rightarrow \tilde{\chi}_6^0 \tilde{\chi}_1^\pm$, $\tilde{\chi}_2^0 \tilde{\chi}_1^\pm$, $\tilde{\chi}_1^0 \tilde{\chi}_2^0$, $\tilde{\chi}_4^0 \tilde{\chi}_6^0$ and $pp \rightarrow \tilde{\chi}_2^0 \tilde{\chi}_4^0$ (hundreds of fb). In Scenario B the dominant decays are into neutralino pairs, again in order: $pp \rightarrow \tilde{\chi}_3^0 \tilde{\chi}_4^0$, $\tilde{\chi}_5^0 \tilde{\chi}_6^0$, $\tilde{\chi}_1^0 \tilde{\chi}_2^0$, $\tilde{\chi}_1^0 \tilde{\chi}_6^0$, while the decays into charginos are dominated by $pp \rightarrow \tilde{\chi}_5^0 \tilde{\chi}_1^\pm$. In Scenario C, the dominant decay is $pp \rightarrow \tilde{\chi}_2^0 \tilde{\chi}_1^\pm$ while all others are negligible. To sum up, cross sections in Scenario A are dominated by chargino-neutralino production, while in Scenario B the cross sections are dominated by production of two neutralinos, while for both scenarios the cross section for lightest chargino pair production is large. Scenario C is dominated by a single chargino-neutralino decay $\tilde{\chi}_2^0 \tilde{\chi}_1^\pm$, chosen to enhance the three-lepton signal.

In Table III, we also included the relic density of the dark matter for all scenarios. This

TABLE I. *The benchmark points for the $U(1)'$ model (Scenario A, Scenario B and Scenario C).*

Parameters	Scenario A	Scenario B	Scenario C
$\tan \beta$	≈ 1	≈ 1	≈ 1
Q'_Q	-2	0	0
$\mu(\mu_{eff})$	139.05	282.8	265
h_ν	1	1	1
h_s	0.75	0.8	0.8
\bar{h}_s	0.075	0.1	0.1
A_s	195.5	557.7	557.7
$A_{\bar{s}}$	195.5	557.7	557.7
v_{s1}	1782.4	100	100
v_{s2}	1782.4	3000	3000
v_{s3}	1778.1	100	100
$R_{Y'}$	12	0.8	5
$R_{YY'}$	10	8	4.8
$M_{\tilde{\nu}_{eR}}$	600	1700	1700
$M_{\tilde{\nu}_{\mu R}}$	650	1750	1750
$M_{\tilde{\nu}_{\tau R}}$	700	1800	1800
M_1	-100	100	-400
M_2	-800	700	212
M_3	1000	1000	1000
M_{L1}	250	600	573
M_{E1}	260	300	300
M_{Q1}	950	1000	1000
M_{U1}	900	1900	1900
M_{D1}	890	1200	1200
M_{L2}	250	600	573
M_{E2}	260	300	300
M_{Q2}	950	1000	1000
M_{U2}	900	1900	1900
M_{D2}	890	1200	1200
M_{L3}	240	575	573
M_{E3}	250	275	275
M_{Q3}	850	1400	1400
M_{U3}	800	2100	2100
M_{D3}	880	1500	1500
M_{SS1}^2	-382.3	$(306)^2$	$(306)^2$
M_{SS2}^2	-382.3	$(56)^2$	$(56)^2$
M_{S1S2}^2	0	0	0
A_t	-697.75	-697.75	-697.75
A_b	-959.66	-959.66	-959.66
A_τ	-138.7	-138.7	-138.7

TABLE II. *The mass spectra for the benchmark points given in Table I for the secluded $U(1)'$.*

Masses	Scenario A	Scenario B	Scenario C
$m_{Z'}$	2015.8	1414.7	1412.4
$m_{\tilde{\chi}_1^0}$	72.1	50.9	56.9
$m_{\tilde{\chi}_2^0}$	78.5	71.5	154.6
$m_{\tilde{\chi}_3^0}$	94.2	211.4	154.9
$m_{\tilde{\chi}_4^0}$	151.7	212.5	211.4
$m_{\tilde{\chi}_5^0}$	188.9	278.8	212.7
$m_{\tilde{\chi}_6^0}$	217.5	339.6	318.7
$m_{\tilde{\chi}_7^0}$	806.7	714.7	324.5
$m_{\tilde{\chi}_8^0}$	1771.9	1577.4	1435.7
$m_{\tilde{\chi}_9^0}$	2901.3	1673.9	3654.1
$m_{\tilde{\chi}_1^\pm}$	145.8	268.1	154.6
$m_{\tilde{\chi}_2^\pm}$	806.7	714.7	322.5
$m_{\tilde{e}_L}$	259.1	217.3	120.3
$m_{\tilde{e}_R}$	249.5	1155.7	1157.5
$m_{\tilde{\mu}_L}$	259.1	217.3	120.3
$m_{\tilde{\mu}_R}$	249.5	1155.7	1157.5
$m_{\tilde{\tau}_1}$	239.0	133.7	120.3
$m_{\tilde{\tau}_2}$	249.5	1149.4	1151.3
$m_{\tilde{\nu}_e}$	258.9	215.0	116.0
$m_{\tilde{\nu}_\mu}$	258.9	215.0	116.0
$m_{\tilde{\nu}_\tau}$	249.3	129.8	116.0
$m_{\tilde{\nu}_{eR}}$	597.9	643.3	636.6
$m_{\tilde{\nu}_{\mu R}}$	648.1	765.7	760.1
$m_{\tilde{\nu}_{\tau R}}$	698.2	874.0	869.0
$m_{H_1^0}$	79.6	136.3	136.8
$m_{H_2^0}$	131.3	178.0	182.1
$m_{H_3^0}$	138.0	313.3	312.9
$m_{H_4^0}$	167.0	552.0	533.9
$m_{H_5^0}$	213.1	790.3	773.2
$m_{H_6^0}$	2020.6	1418.8	1416.3
$m_{A_1^0}$	7.4	129.7	132.5
$m_{A_2^0}$	64.8	309.6	308.1
$m_{A_3^0}$	235.4	582.2	565.9
$m_{A_4^0}$	259.5	793.5	776.2
m_{H^\pm}	209.0	553.6	535.1

TABLE III. Total cross sections for production of $\tilde{\chi}_i^0 \tilde{\chi}_j^0$, $\tilde{\chi}_i^0 \tilde{\chi}_j^\pm$ and $\tilde{\chi}_i^\pm \tilde{\chi}_j^\mp$ and the relic density Ω_{DM} values for the three scenarios considered.

Observables	Scenario A	Scenario B	Scenario C
$\sigma(\text{pp} \rightarrow \tilde{\chi}_1^0 \tilde{\chi}_2^0)/\text{fb}$	238	628	≈ 0
$\sigma(\text{pp} \rightarrow \tilde{\chi}_1^0 \tilde{\chi}_6^0)/\text{fb}$	≈ 0	169	≈ 0
$\sigma(\text{pp} \rightarrow \tilde{\chi}_2^0 \tilde{\chi}_2^0)/\text{fb}$	55	≈ 0	≈ 0
$\sigma(\text{pp} \rightarrow \tilde{\chi}_2^0 \tilde{\chi}_4^0)/\text{fb}$	153	≈ 0	≈ 0
$\sigma(\text{pp} \rightarrow \tilde{\chi}_3^0 \tilde{\chi}_4^0)/\text{fb}$	≈ 0	1146	≈ 0
$\sigma(\text{pp} \rightarrow \tilde{\chi}_4^0 \tilde{\chi}_6^0)/\text{fb}$	225	≈ 0	≈ 0
$\sigma(\text{pp} \rightarrow \tilde{\chi}_5^0 \tilde{\chi}_6^0)/\text{fb}$	≈ 0	780	≈ 0
$\sigma_{\text{TOT}}(\text{pp} \rightarrow \tilde{\chi}_i^0 \tilde{\chi}_j^0)/\text{fb}$	$< 743 >$	$< 4827 >$	≈ 0
$\sigma(\text{pp} \rightarrow \tilde{\chi}_2^0 \tilde{\chi}_1^\pm)/\text{fb}$	279	≈ 0	2170
$\sigma(\text{pp} \rightarrow \tilde{\chi}_4^0 \tilde{\chi}_1^\pm)/\text{fb}$	1037	≈ 0	≈ 0
$\sigma(\text{pp} \rightarrow \tilde{\chi}_5^0 \tilde{\chi}_1^\pm)/\text{fb}$	≈ 0	113	≈ 0
$\sigma(\text{pp} \rightarrow \tilde{\chi}_6^0 \tilde{\chi}_1^\pm)/\text{fb}$	369	62	≈ 0
$\sigma_{\text{TOT}}(\text{pp} \rightarrow \tilde{\chi}_i^\pm \tilde{\chi}_j^0)/\text{fb}$	$< 1739 >$	$< 235 >$	2368
$\sigma(\text{pp} \rightarrow \tilde{\chi}_1^+ \tilde{\chi}_1^-)/\text{fb}$	693	1120	≈ 0
$\sigma_{\text{TOT}}(\text{pp} \rightarrow \tilde{\chi}_i^\pm \tilde{\chi}_j^\mp)/\text{fb}$	$< 694 >$	$< 1166 >$	≈ 0
$\Omega_{\text{DM}} h^2$	0.102	0.115	0.108

calculation is performed including the model files from `CalcHEP` into the `MicrOmegas` package [31]. All the numbers obtained are within the 1σ range of the WMAP result [25] obtained from the Sloan Digital Sky Survey [32]

$$\Omega_{\text{DM}} h^2 = 0.111_{-0.015}^{+0.011}. \quad (11)$$

The relic density of dark matter $\Omega_{\text{DM}} h^2$ is very sensitive to the parameter $R_{Y'} \equiv M_{\tilde{Y}'} / M_{\tilde{Y}}$ from Table I. In Table II, the lightest neutralino $\tilde{\chi}_1^0$ is the LSP, with masses 72.1 GeV, 50.9 GeV and 56.9 GeV for Scenario A, Scenario B and Scenario C, respectively.

The decay channels of heavy neutralinos depend on their masses and the masses and couplings of other sparticles and Higgs bosons. A sufficiently heavy neutralino can decay via tree-level two-body channels containing a Z, (W) or a Higgs boson, and a lighter neutralino

and a sfermion-fermion pair.

B. Chargino and Neutralino Signals at the LHC

After defining the benchmark points for $U(1)'$ and calculating the the relic density, we analyze the signals at LHC from neutralino and chargino production processes. Fig. 1 shows the Feynman diagrams contributing to the chargino and neutralino production in the secluded $U(1)'$ model. We leave the diagrams for the characteristic decay patterns in the three scenarios for the Appendix B.

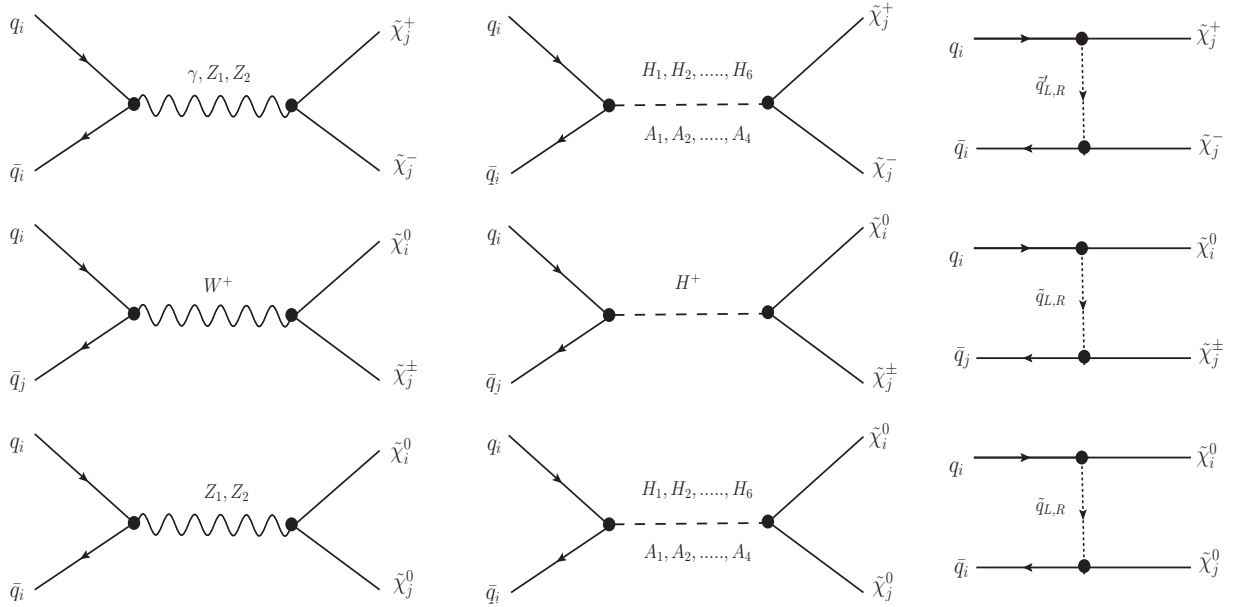


FIG. 1. The Feynman diagrams for the production of the chargino and neutralino in the secluded- $U(1)'$ model. The top row shows chargino production only, the middle row the associated chargino-neutralino, and the bottom row shows the neutralino pair production.

To determine and classify all possible signals for the three scenarios we need to look at the decay topology of these particles. We classify signals according to the final number of leptons present in the signal events. We impose the following basic cuts (we call the set *cut-1*) to suppress the SM background, where relevant:

- (i) Each isolated charged lepton (electron or muon) has a minimum transverse momentum $p_T(\ell) > 15$ GeV;
- (ii) The missing transverse energy must be larger than $\cancel{E}_T > 100$ GeV;

- (iii) If two leptons or more are produced, they are constrained to be in the central region by the condition on pseudorapidity $|\eta| < 2$;
- (iv) The cone size between two charged leptons $\Delta R_{\ell\ell} \geq 0.4$, where $\Delta R_{\ell\ell}$ is defined in the pseudorapidity-azimuthal angle plane as $\Delta R_{\ell\ell} = (\Delta\eta^2 + \Delta\phi^2)^{1/2}$.

TABLE IV. *The SM background cross in fb sections after cut-1 and cut-2.*

Background [fb]	Cut	$1\ell 2j \cancel{E}_T$	$2\ell 2j \cancel{E}_T$	$3\ell 0j \cancel{E}_T$
ZZ	<i>cut-1</i>	—	4.3	—
	<i>cut-2</i>	—	0	—
WW	<i>cut-1</i>	156.9	11.2	—
	<i>cut-2</i>	1.4	0.3	—
WZ	<i>cut-1</i>	98.3	—	4.5
	<i>cut-2</i>	0.4	—	0.4
$t\bar{t}$	<i>cut-1</i>	2502.9	205.5	—
	<i>cut-2</i>	6.7	0	—
Total :	<i>cut-1</i>	2758.1	221.0	4.5
	<i>cut-2</i>	8.5	0.3	0.4

In Table IV we list the SM background contributions (given along rows) to the cross sections of the signals (given in between the 4th to 6th columns of Table V) after the *cut-1* set is imposed, including as well as the numbers after a second more restrictive set, called *cut-2*, is considered. We found that the set *cut-2* is needed to reduce the SM background further, where we modified only the missing transverse energy \cancel{E}_T cut as compared to the first set. We impose:

- $\cancel{E}_T > 500$ GeV for the scenarios A and B, and $\cancel{E}_T > 200$ GeV for the scenario C.

As can be seen from the numbers in Table IV, after imposing the *cut-2*, as compared to the ones for the *cut-1*, the signal cross sections is reduced on average to around 3 parts in thousands for the monolepton signal, around 1 part in thousands for the dilepton signal, and around 9 percent for the trilepton signal.

We use the following formula for the significance of the signals (signal-to-background):

$$\beta_{\alpha}^{ij}(r) = \frac{N_{\alpha}^{ij}}{\sqrt{N_{SM}^{bg} + r \sum_{k,l \neq i,j} N_{\alpha}^{kl}}} \quad (12)$$

where N are the number of events and $\alpha = A, B, C$ represent Scenarios A, B, and C, respectively. The indices $i, j = n, c$ run over the chargino, neutralino states contributing to the signals. The parameter r can take two values, 0 or 1. The case with $r = 0$ corresponds to the significance with no sizable contribution to the background from the $U(1)'$ model. Whenever there is a need to consider any contamination from the other $U(1)'$ channels, $r = 1$ is taken.

The possible contributions to the background in the signal regions come from the SM processes. In the $1\ell + jets + \cancel{E}_T$ case, the background arises from $pp \rightarrow WZ$, $pp \rightarrow WW$ and $pp \rightarrow \bar{t}t$. The processes $pp \rightarrow ZZ$, $pp \rightarrow WW$ and $pp \rightarrow \bar{t}t$ can yield background for the $2\ell + jets + \cancel{E}_T$ mode. And the process $pp \rightarrow WZ$ can be the background for the $3\ell + 0jets + \cancel{E}_T$ decay mode. Since those background channels can have large cross sections, some additional cuts need to be implemented as mentioned above.

In Table V we list the cross sections obtained after we perform both *cut-1* and *cut-2* for the signals in Scenarios A, B and C. The numbers for the signal significance show that events in Scenario A have no chance to be observed. For Scenario B, only monolepton signals generated via chargino pair seem to be promising since they have signal significance greater than 5 events after the first *cut-1* set. A better option is the trilepton signal with no jets from Scenario C. The signal significance with $r = 1$ is not calculated since there are no other channels giving significant trilepton signals with no jets.

We are interested in signals with leptons in the final state, as these would be clear to identify at the LHC. We analyzed the signal with missing energy only $0\ell + jets + \cancel{E}_T$, but unfortunately, although strong, this signal is completely overwhelmed by the background, mostly Drell-Yan production $pp \rightarrow ZZ$ and $pp \rightarrow WW$. Cuts for $p_T^{jet} > 20$ GeV, for $N_{jet} > 2$, $E_T^{\text{sum}} > 1.2$ TeV, and $\cancel{E}_T > 1$ TeV may yield some signal, but it would still be difficult to isolate and distinguish securely from background.

We thus concentrate our analysis on monolepton, dilepton and trilepton final states, accompanied by jets (except for the trilepton signal). We note that in the rest of the signal simulations we used the software PGS 4 [33] to include LHC detector effects. PGS 4 uses a jet algorithm which assumes that jets are confined in a cone with diameter $\Delta R_{jj} = 0.5$,

TABLE V. The cross sections for signal events and signal to background significance after the *cut-1* and *cut-2* with an integrated luminosity of 100 fb^{-1} . See the text for the definition of $\beta_{\alpha}^{ij}(r)$. $\beta_{\alpha}^{ij}(0)$ is the significance with no contamination from others channels.

Signal	Channel	Cut	SA[fb]	SB[fb]	SC[fb]	$\beta_A^{ij}(0)$	$\beta_B^{ij}(0)$	$\beta_C^{ij}(0)$	$\beta_A^{ij}(1)$	$\beta_B^{ij}(1)$
<i>1ℓ2j \cancel{E}_T</i>										
	$\tilde{\chi}_i^+ \tilde{\chi}_j^-$	<i>cut-1</i>	3.4	51.9	—	0.6	10.0	—	0.6	9.9
		<i>cut-2</i>	0.3	12.5	—	1.0	43.0	—	1.0	42.6
	$\tilde{\chi}_i^0 \tilde{\chi}_j^0$	<i>cut-1</i>	—	0.3	—	—	0.06	—	—	0.06
		<i>cut-2</i>	—	0.03	—	—	0.1	—	—	0.07
	$\tilde{\chi}_i^0 \tilde{\chi}_j^{\pm}$	<i>cut-1</i>	7.6	2.0	—	1.5	0.4	—	1.4	0.4
		<i>cut-2</i>	0.05	0.07	—	0.2	0.2	—	0.2	0.2
<i>2ℓ2j \cancel{E}_T</i>										
	$\tilde{\chi}_i^+ \tilde{\chi}_j^-$	<i>cut-1</i>	0.2	0.9	—	0.1	0.6	—	0.1	0.6
		<i>cut-2</i>	0.03	0.1	—	0.5	1.8	—	0.5	1.5
	$\tilde{\chi}_i^0 \tilde{\chi}_j^0$	<i>cut-1</i>	0.07	1.7	—	0.05	1.1	—	0.05	1.1
		<i>cut-2</i>	0.01	0.12	—	0.2	2.2	—	0.2	1.9
	$\tilde{\chi}_i^0 \tilde{\chi}_j^{\pm}$	<i>cut-1</i>	0.01	0.4	—	0.0	0.3	—	0.0	0.3
		<i>cut-2</i>	0	0	—	0.0	0.0	—	0.0	0.0
<i>3ℓ0j \cancel{E}_T</i>										
	$\tilde{\chi}_i^0 \tilde{\chi}_j^{\pm}$	<i>cut-1</i>	—	—	55.0	—	—	260.0	—	—
		<i>cut-2</i>	—	—	10.0	—	—	156.4	—	—

together with a hadronic calorimeter energy resolution as $\sigma(E_T^{\text{jet}}) = 0.8\sqrt{E_T^{\text{jet}}}$.

1. The Monolepton Signal: $1\ell + \text{jets} + \cancel{E}_T$

We analyze first the case of a single charged lepton with at least two jets in the signal. In Fig. 2 we plot the relevant distributions \cancel{E}_T , E_T^{sum} , $p_T(\ell)$, N_{jet} and p_T^{jet} distributions of the $1\ell + 2j + \cancel{E}_T$ signal at 14 TeV with integrated luminosity $\mathcal{L} = 100 \text{ fb}^{-1}$, for Scenario A. The dominant signals $\tilde{\chi}_1^+ \tilde{\chi}_1^-$ and $\tilde{\chi}_1^{\pm} \tilde{\chi}_i^0$ show different distributions in \cancel{E}_T , E_T^{sum} . The decay into

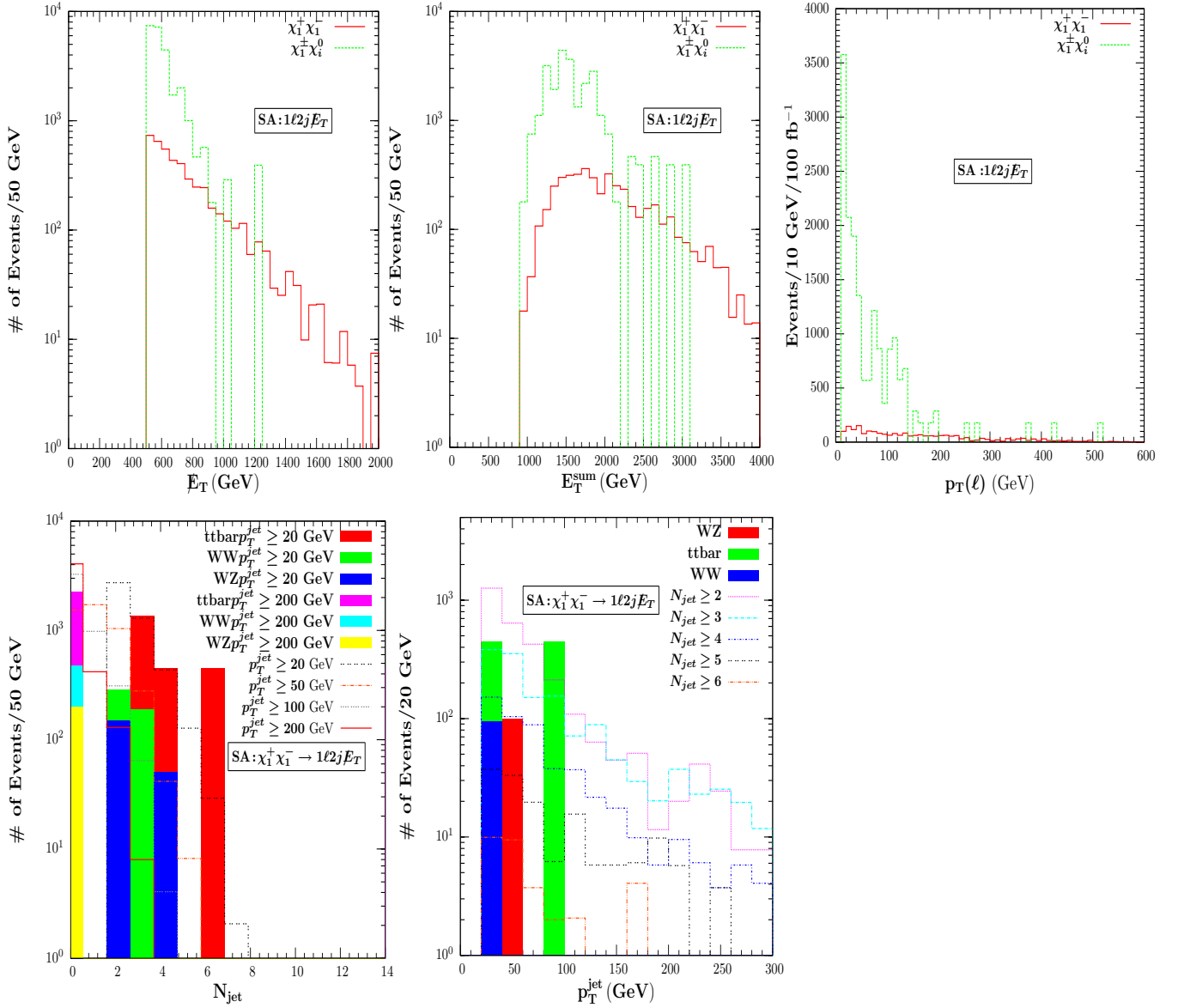


FIG. 2. (color online). The \cancel{E}_T , E_T^{sum} , $p_T(\ell)$, N_{jet} and p_T^{jet} distributions of the $1\ell + 2j + \cancel{E}_T$ signal at 14 TeV with integrated luminosity $\mathcal{L} = 100 \text{ fb}^{-1}$, for Scenario A.

chargino pairs has a tail at large \cancel{E}_T , E_T^{sum} , while the chargino-neutralino signal peaks at low \cancel{E}_T , E_T^{sum} . In $p_T(\ell)$ the two-charginos signal is not visible, while the chargino-neutralino signal peaks at low $p_T(\ell) < 100 \text{ GeV}$. The number of events per bin-size as a function of the number of jets is completely overwhelmed by backgrounds ($t\bar{t}$, WW and WZ), while as a function of p_T^{jet} , secluded $U(1)'$ events are visible for $p_T^{\text{jet}} > 100 \text{ GeV}$.

The same analysis for Scenario B, shown in Fig. 3, yields non-negligible distributions for $\tilde{\chi}_1^+ \tilde{\chi}_1^-$, $\tilde{\chi}_1^\pm \tilde{\chi}_i^0$ and $\tilde{\chi}_i^0 \tilde{\chi}_j^0$ (the last being the smallest). The chargino pair decay is again

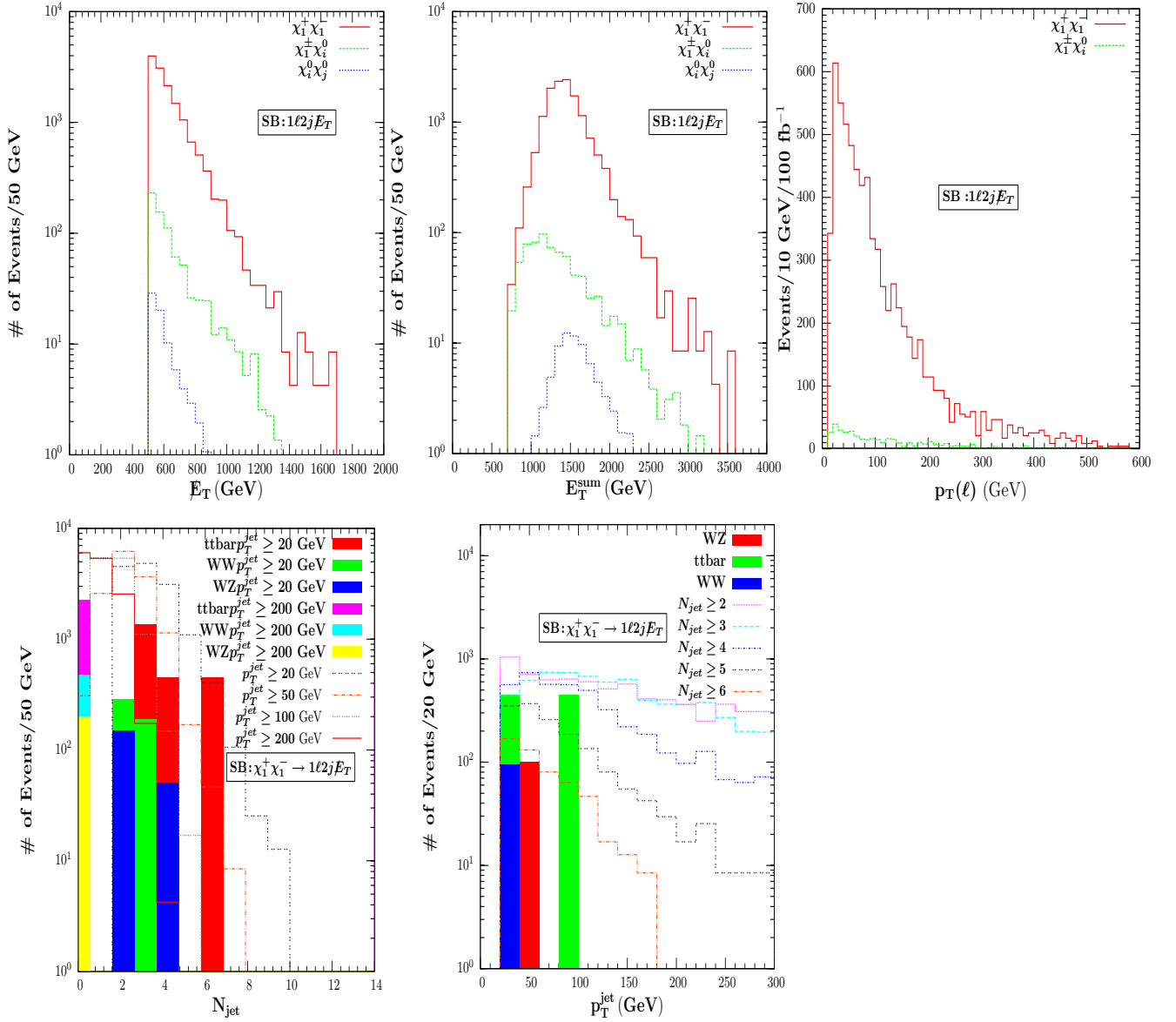


FIG. 3. (color online). The \cancel{E}_T , E_T^{sum} , $p_T(\ell)$, N_{jet} and p_T^{jet} distributions of the $1\ell + 2j + \cancel{E}_T$ signal at 14 TeV with integrated luminosity $\mathcal{L} = 100 \text{ fb}^{-1}$, for Scenario B.

dominant but its tail at large \cancel{E}_T , E_T^{sum} , falls more abruptly than that in Scenario A, while the chargino-neutralino signal peaks at low \cancel{E}_T , E_T^{sum} . Unlike in Scenario A, in the $p_T(\ell)$ distribution the two chargino signal is dominant, and significant for $p_T(\ell) \leq 150 - 200 \text{ GeV}$, while the other two are not visible. The number of events per bin-size as a function of the number of jets is, as in Scenario A, completely overwhelmed by backgrounds ($t\bar{t}$, WW and WZ), while as a function of p_T^{jet} , secluded $U(1)'$ events are visible for $p_T^{\text{jet}} > 100 \text{ GeV}$, where the number of events per bin size exceeds those in Scenario A by an order of magnitude.

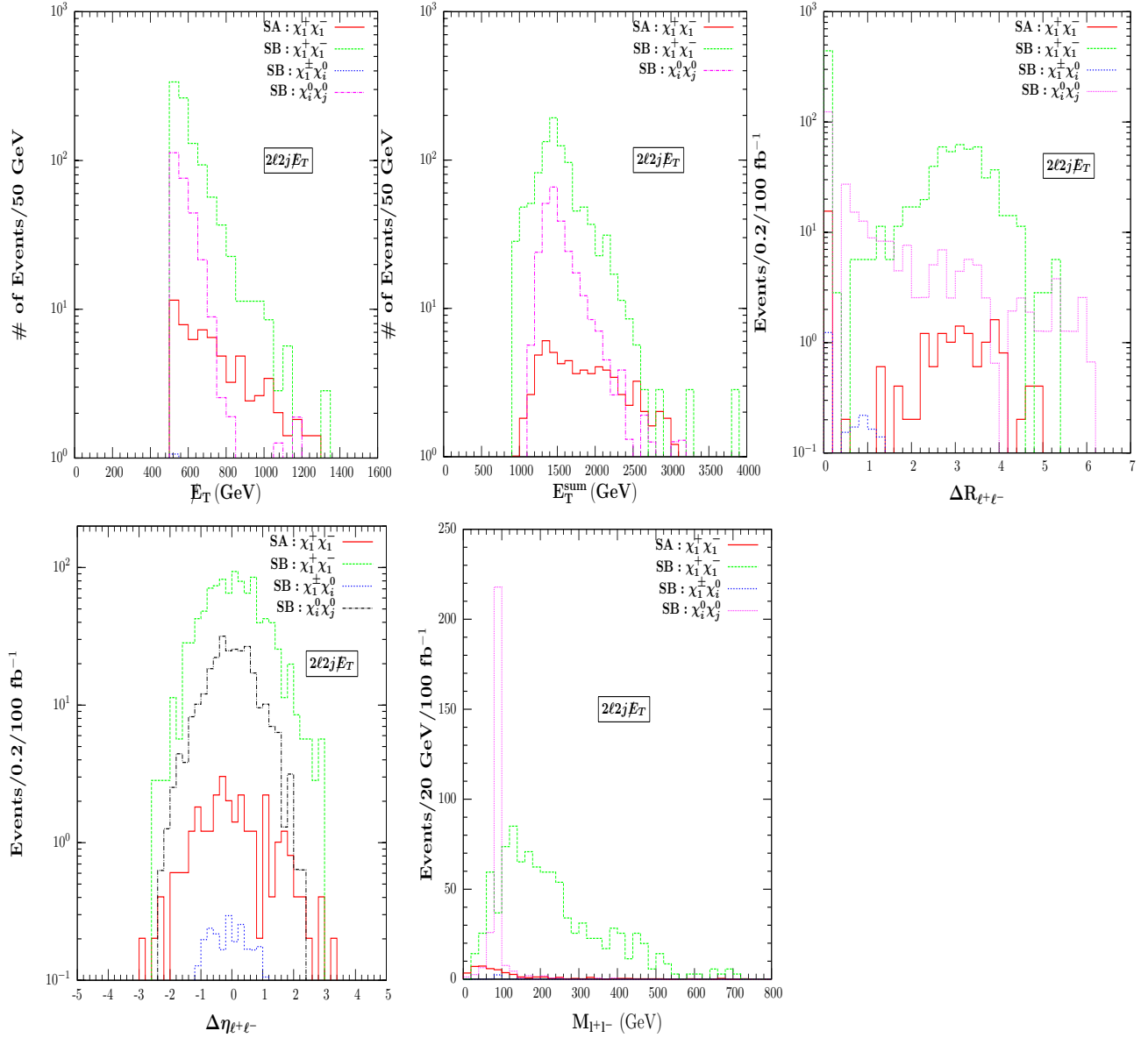


FIG. 4. (color online). The \cancel{E}_T , E_T^{sum} , $\Delta R_{\ell+\ell-}$ and $\Delta \eta_{\ell+\ell-}$ and the invariant mass distributions of the $2\ell + 2j + \cancel{E}_T$ signal at 14 TeV with integrated luminosity $\mathcal{L} = 100 \text{ fb}^{-1}$, for Scenario A and Scenario B.

Given the abundance of the neutralinos in the signal, we expect some enhancement in the total signal (cross section) with respect to the MSSM.

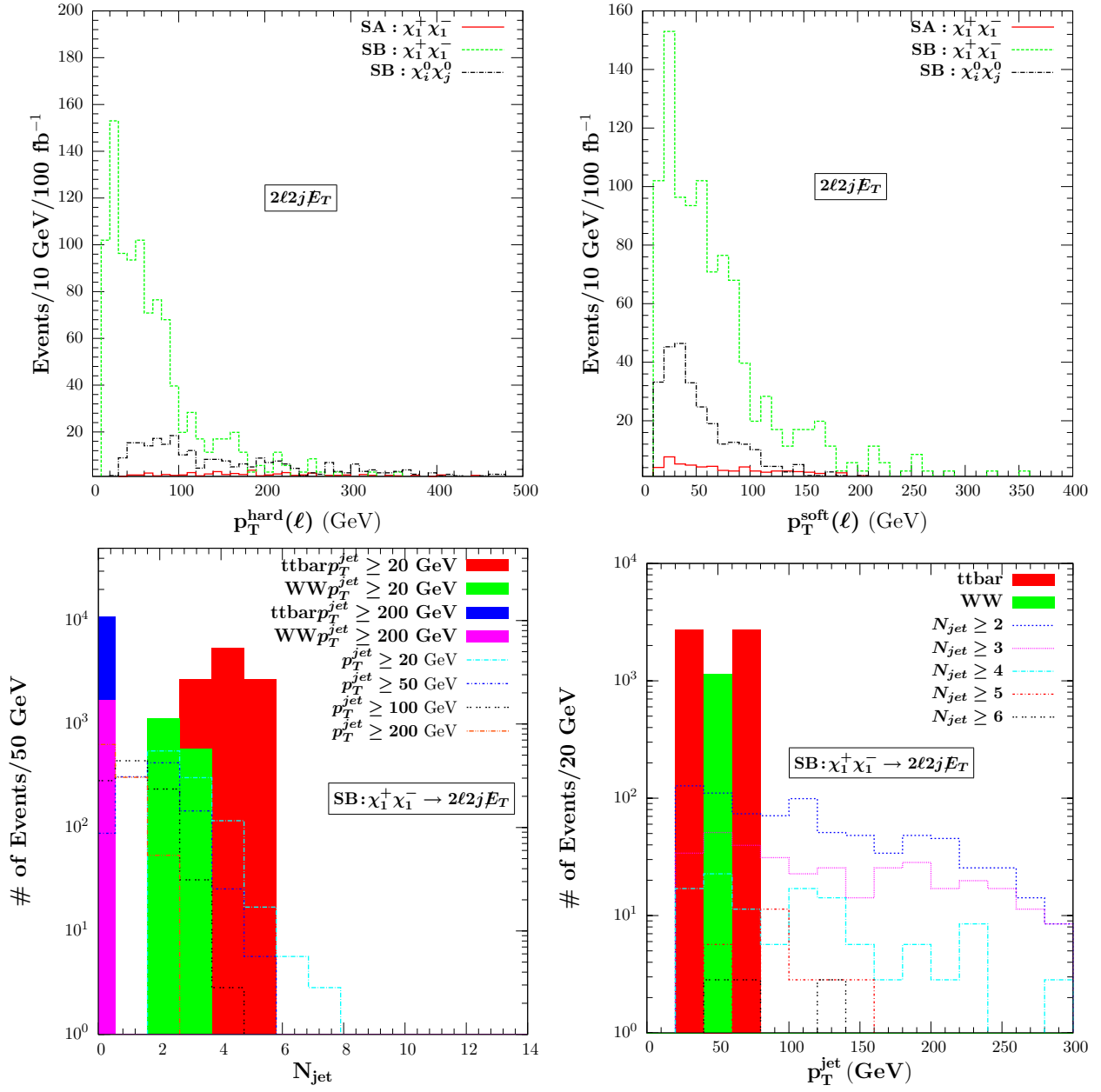


FIG. 5. (color online). The p_T distribution for Scenario A and B, and the N_{jet} and p_T^{jet} distributions of the $2\ell + 2j + \cancel{E}_T$ ($\tilde{\chi}_i^+ \tilde{\chi}_j^-$) signal at 14 TeV with integrated luminosity $\mathcal{L} = 100 \text{ fb}^{-1}$, for Scenario B. For Scenario A, the background is too large and completely obliterates the signal.

2. The Dilepton Signal: $2\ell + jets + \cancel{E}_T$

We analyze the $2\ell + jets + \cancel{E}_T$ in a similar fashion to the $1\ell + jets + \cancel{E}_T$ presented in the previous subsection. The main results are shown in Fig. 4, where we plot the \cancel{E}_T , E_T^{sum} , $\Delta R_{\ell+\ell^-}$ and $\Delta \eta_{\ell+\ell^-}$ and the invariant mass distributions of the $2\ell + 2j + \cancel{E}_T$ signal at 14 TeV

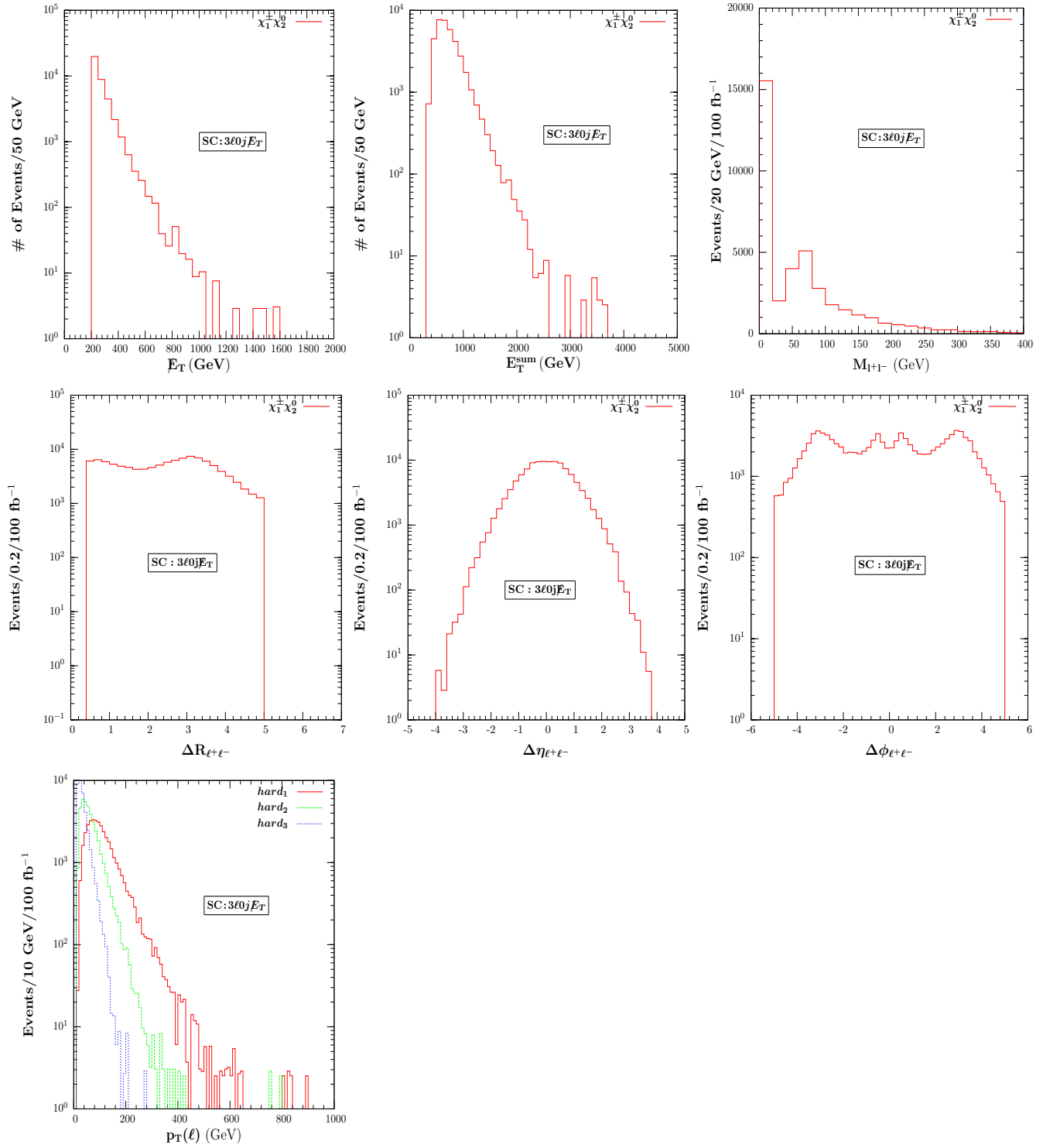


FIG. 6. (color online). The \cancel{E}_T , E_T^{sum} , invariant mass, $\Delta R_{\ell^+\ell^-}$, $\Delta \eta_{\ell^+\ell^-}$, $\Delta \phi_{\ell^+\ell^-}$ and p_T distributions of the $3\ell + 0j + \cancel{E}_T$ signal at 14 TeV with integrated luminosity $\mathcal{L} = 100 \text{ fb}^{-1}$, for Scenario C.

with integrated luminosity $\mathcal{L} = 100 \text{ fb}^{-1}$, for Scenario A and Scenario B; and in Fig. 5 where we give the p_T distribution for Scenario A and B, and the N_{jet} and p_T^{jet} distributions of the $2\ell + 2j + \cancel{E}_T$ ($\tilde{\chi}_i^+ \tilde{\chi}_j^-$) signal at 14 TeV with integrated luminosity $\mathcal{L} = 100 \text{ fb}^{-1}$, for Scenario B, where the signal survives background cuts. For Scenario A, the background is too large and completely obliterates the signal.

For the \cancel{E}_T and E_T^{sum} graphs, the dominant signals are $\tilde{\chi}_1^+ \tilde{\chi}_1^-$ in Scenario A, and $\tilde{\chi}_1^+ \tilde{\chi}_1^-$ and $\tilde{\chi}_i^0 \tilde{\chi}_j^0$ in Scenario B (where the last two give an enhanced number of events over the signal in Scenario A). Note however that the number of events per bin decreases by roughly an order of magnitude with respect to the $1\ell + jets + \cancel{E}_T$ signal. The signal peaks around 600 GeV for \cancel{E}_T and 1500 GeV for E_T^{sum} . Looking at angular variables for the two-lepton final signal, such as the cone size between two charged leptons, the pseudorapidity and the two-lepton invariant mass distinguish between the signals. The chargino pair production in Scenario B gives the largest signal in cone size and pseudorapidity distributions, peaked respectively around 3 and 0; while in the two-lepton invariant mass distribution M_{l+l-} the Scenario B signal $\tilde{\chi}_i^0 \tilde{\chi}_j^0$ peaks sharply around 80 GeV, and is negligible elsewhere, and for Scenario B for $\tilde{\chi}_1^+ \tilde{\chi}_1^-$ the number of events per bin size is smaller by a factor of about 3, but the signal is visible round $M_{l+l-} \sim 50 - 200 \text{ GeV}$. Looking at the distributions of both p_T^{hard} and p_T^{soft} in Fig. 5, the only visible signal is the chargino-pair production $\tilde{\chi}_1^+ \tilde{\chi}_1^-$ in Scenario B, which peaks for both distributions around 50 GeV. As for the $1\ell + jets + \cancel{E}_T$ case, the number of events per bin-size as a function of the number of jets N_{jet} falls under the backgrounds from $t\bar{t}$, WW and ZZ , while as a function of p_T^{jet} , secluded $U(1)'$ events are visible for $p_T^{jet} > 80 \text{ GeV}$, and the events with $N_{jet} \geq 2$ dominate. From \cancel{E}_T and E_T^{sum} graphs, it is apparent that the dilepton distribution shows more deviation from the SM than the monolepton, given the importance of $\tilde{\chi}_i^0 \tilde{\chi}_j^0$ signal.

3. The Trilepton Signal: $3\ell + 0jets + \cancel{E}_T$

Neither Scenario A nor Scenario B give any significant signals for the trilepton signal, consider to be the golden signature for supersymmetry. For these final states, one expects events containing three hard isolated leptons (and \cancel{E}_T), with no jets, and small SM backgrounds. To highlight this signal, we have set up another alternative, Scenario C, where the dominant signal is $\tilde{\chi}_1^\pm \tilde{\chi}_2^0$, yielding $\ell_i^\pm \ell_j^+ \ell_j^- + \cancel{E}_T$. We generated about 2.7×10^5 to enhance

the event to background ratio.

We present our results in Fig. 6, together with the dominant SM background coming from WZ . For the modified cut $\cancel{E}_T > 200$ GeV (*cut-2*), it is clear that this signal is background-free and will be distinguished by measurement of both \cancel{E}_T and E_T^{sum} , and of the angular correlations, as the cone size between two charged leptons, the pseudorapidity and the two-lepton azimuthal angle. For \cancel{E}_T and E_T^{sum} , the signal is strong till 800 and 2000 GeV, respectively. In the two-lepton invariant mass, the signal is strong for $M_{l+l-} = 0 - 20$ GeV and less so in the 50 – 80 GeV region. We also show the $p_T(\ell)$ for the three hard leptons in the last panel, distinguished by their increasingly broader peaks. This signal could be observed at the 14 TeV LHC, as more than 100 events per year would be observed. This signal, though promising, may not be able to distinguish the model from MSSM, where the trilepton signal is also dominated by $\tilde{\chi}_1^\pm \tilde{\chi}_2^0$ production, and where similar cross sections are expected [23].

IV. SUMMARY AND CONCLUSION

We have studied the production of neutralinos and charginos at the LHC in the context of the secluded $U(1)'$, in which singlet fields are added to the ordinary extra $U(1)$ supersymmetric models to stabilize the $Z - Z'$ mass splitting. The model has five additional neutralinos (in addition to the four in MSSM), which could enhance the signals observed at the LHC. In fact, if the additional Higgs singlets are heavy, analyzing the neutralino sector would be a more promising test of the secluded sector of the model. We perform the analysis for LHC operating at 14 TeV with integrated luminosity $\mathcal{L} = 100 \text{ fb}^{-1}$.

We classify and analyze the final signals based on the number of leptons emitted, and look at final states with $1\ell + jets + \cancel{E}_T$, $2\ell + jets + \cancel{E}_T$ and $3\ell + 0jets + \cancel{E}_T$. There are very few events generated with more than three leptons in the final states in this model, and thus these are not likely to be seen at the LHC, even at 14 TeV. For each signal, we study a parameter space where the signals could be enhanced. In two of the Scenarios, A and B, the largest cross section is obtained for the production of the lightest chargino pair, or the lightest chargino with neutralinos. Both can generate $10^2 - 10^3$ events per energy bin, and seem most promising to be observed in \cancel{E}_T and E_T^{sum} plots, or in p_T^{jet} , with a cut $p_T^{\text{jet}} > 80 - 100$ GeV, to enhance the signal to background response. Increasing the

number of leptons in the final state produces fewer events, however with a reduction in the background as well. We found that for the $2\ell + jets + \cancel{E}_T$ in Scenario A, the background completely overwhelms the signal, while Scenario B remains promising. For highlighting the $3\ell + 0jets + \cancel{E}_T$ scenario, we analyzed another region of the parameter space, Scenario C, where the dominant cross section is to the lightest chargino and second lightest neutralino, resulting in a final $3\ell + 0jets + \cancel{E}_T$ final state. We find that plots for events yield observable results, and with judicious cuts ($\cancel{E}_T > 200$ GeV) they are almost background-free, and could yield as many as 10^4 events per energy bin at the LHC.

Given the pressure put on the constrained and phenomenological MSSM (CMSSM and pMSSM) by present measurements at the LHC, the analysis presented here provides a map of possible signals in neutralino production of physics beyond MSSM, which should be easily confirmed or ruled out at 14 TeV. If $U(1)'$ is the correct supersymmetric scenario, the difference with MSSM will not likely be seen in the trilepton signal, but will manifest itself in the $1\ell + jets + \cancel{E}_T$ and $2\ell + jets + \cancel{E}_T$ signal, where the cross sections (and the correlated number of events) should be above what one expects in the minimal model.

V. ACKNOWLEDGMENTS

M.F. would like to thank Benjamin Fuks for his comments and for many discussions on the topic of chargino and neutralino production. The work of M.F. is supported in part by NSERC under grant number SAP105354. The research of L. S. is supported in part by The Council of Higher Education (YOK) of Turkey.

Appendix A: The Composition of the Neutralinos

In this Appendix we give, in Table VI, the Bino, Zino', Wino, Higgsino and Singlino components of the physical neutralinos $\tilde{\chi}_i^0, i = 1, 2, \dots, 9$ for Scenario A, Scenario B and Scenario C.

TABLE VI. *The Bino, Wino, Zino', Higgsino and Singlino composition of the neutralinos $\tilde{\chi}_i^0, i = 1, 2, \dots, 9$ for Scenario A, Scenario B and Scenario C.*

Scenario A	$\tilde{\chi}_1^0$	$\tilde{\chi}_2^0$	$\tilde{\chi}_3^0$	$\tilde{\chi}_4^0$	$\tilde{\chi}_5^0$	$\tilde{\chi}_6^0$	$\tilde{\chi}_7^0$	$\tilde{\chi}_8^0$	$\tilde{\chi}_9^0$
\tilde{B}	0.889	-0.004	0.0	-0.151	0.0	0.004	-0.007	0.324	0.283
\tilde{W}^3	0.022	0.0	0.0	0.081	0.0	0.0	0.996	-0.002	0.001
\tilde{H}_d^0	0.131	-0.360	0.0	0.692	0.0	0.607	-0.059	-0.035	-0.018
\tilde{H}_u^0	-0.156	-0.365	0.0	-0.682	0.0	0.605	0.059	0.065	0.039
\tilde{S}	0.025	0.855	0.0	-0.013	0.0	0.514	0.0	-0.042	-0.032
\tilde{Z}'	-0.033	0.0	0.0	-0.004	0.0	0.0	-0.001	-0.604	0.795
\tilde{S}_1	-0.165	0.027	-0.707	0.065	0.577	0.001	-0.001	0.295	0.217
\tilde{S}_2	-0.165	0.027	0.707	0.065	0.577	0.001	-0.001	0.295	0.217
\tilde{S}_3	0.331	-0.055	0.0	-0.130	0.577	-0.003	0.002	-0.589	-0.434
Scenario B									
\tilde{B}	0.349	0.764	0.042	0.007	-0.220	-0.011	-0.021	-0.336	0.359
\tilde{W}^3	-0.017	-0.017	-0.002	0.0	-0.180	0.005	0.983	0.002	0.006
\tilde{H}_d^0	-0.142	0.246	0.007	0.0	0.684	0.658	0.124	-0.032	0.032
\tilde{H}_u^0	-0.312	0.0246	-0.011	-0.002	-0.669	0.651	-0.131	0.072	-0.077
\tilde{S}	0.790	-0.458	0.008	0.002	-0.041	0.377	-0.003	-0.100	0.099
\tilde{Z}'	-0.013	-0.019	0.006	-0.002	0.002	0.002	-0.006	0.701	0.712
\tilde{S}_1	-0.016	-0.020	0.706	0.706	-0.002	0.0	0.0	0.018	-0.022
\tilde{S}_2	0.365	0.377	-0.043	0.028	-0.014	0.010	0.012	0.613	-0.586
\tilde{S}_3	-0.005	-0.001	-0.704	0.707	0.003	0.0	-0.001	-0.035	0.044
Scenario C									
\tilde{B}	0.016	-0.011	-0.639	-0.023	-0.040	0.017	0.005	0.596	0.481
\tilde{W}^3	-0.056	-0.801	0.024	-0.027	0.001	0.593	0.010	-0.007	0.0
\tilde{H}_d^0	-0.217	0.442	-0.049	-0.002	-0.002	0.568	0.654	-0.052	-0.011
\tilde{H}_u^0	-0.329	-0.378	0.104	-0.002	0.004	-0.556	0.645	0.097	0.032
\tilde{S}	0.903	-0.096	-0.090	0.010	-0.003	-0.048	0.392	-0.087	-0.047
\tilde{Z}'	-0.006	-0.009	0.084	0.007	0.004	-0.024	0.001	-0.568	0.817
\tilde{S}_1	-0.007	-0.014	-0.042	0.706	0.705	0.013	0.0	0.021	0.009
\tilde{S}_2	0.157	0.088	0.744	-0.048	0.073	0.107	0.005	0.546	0.308
\tilde{S}_3	-0.001	0.009	-0.074	-0.704	0.703	-0.018	0.0	-0.042	-0.019

Appendix B: Feynman diagrams for decays channels

We list the characteristic decay patterns of chargino and neutralinos in Scenario A, (Fig. 7), Scenario B, (Fig. 8) and Scenario C (Fig. 9).

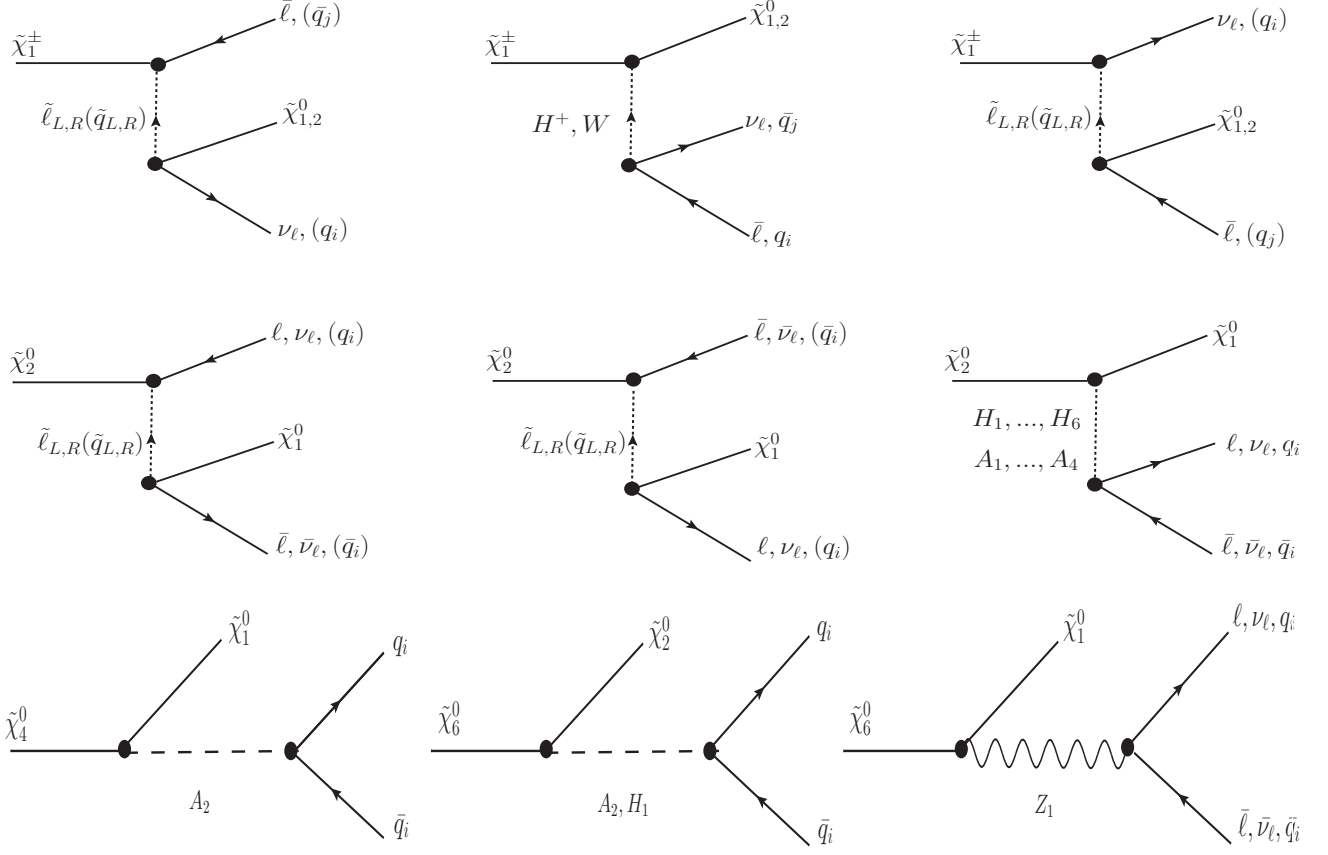


FIG. 7. Generic Feynman diagrams for the decays of the chargino $\tilde{\chi}_1^\pm$ and neutralinos $\tilde{\chi}_2^0$, $\tilde{\chi}_4^0$, and $\tilde{\chi}_6^0$ in Scenario A of the secluded $U(1)'$ model. Here $\tilde{\ell}$ are scalar leptons, H_i , A_j are scalar and pseudoscalar Higgs bosons, and W and Z are gauge bosons.

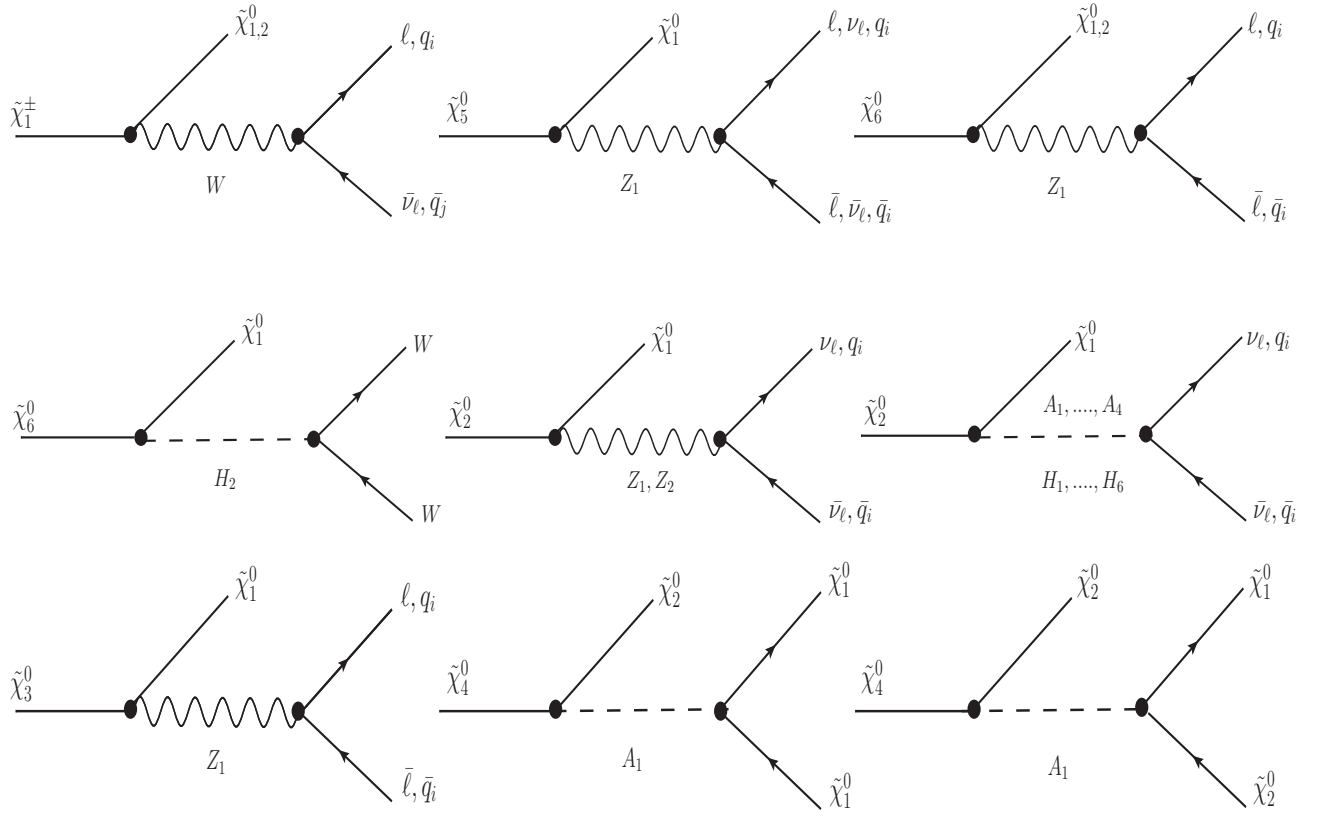


FIG. 8. Generic Feynman diagrams for the decays of the chargino $\tilde{\chi}_1^\pm$ and neutralinos $\tilde{\chi}_i^0$, $i = 2, \dots, 6$ in Scenario B of the secluded $U(1)'$ model. Intermediate particle notation is the same as in Fig. 7.

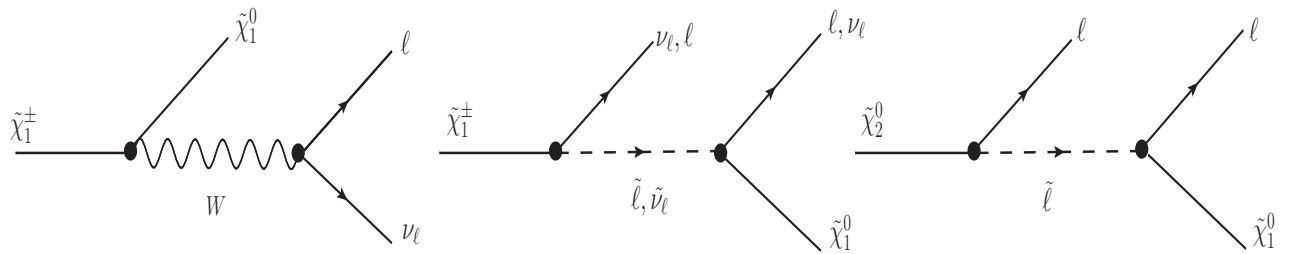


FIG. 9. Generic Feynman diagrams for the decays of the chargino $\tilde{\chi}_1^\pm$ and neutralino $\tilde{\chi}_2^0$ in Scenario C of the secluded $U(1)'$ model. Intermediate particle notation is the same as in Fig. 7, and $\tilde{\nu}_l$ is the scalar neutrino.

-
- [1] G. Aad *et al.* [ATLAS Collaboration], Phys. Lett. B **716**, 1 (2012).
 - [2] S. Chatrchyan *et al.* [CMS Collaboration], Phys. Lett. B **716**, 30 (2012).
 - [3] R. Aaij *et al.* [LHCb Collaboration], arXiv:1211.2674 [Unknown].
 - [4] M. Cvetič and P. Langacker, Phys. Rev. D **54**, 3570 (1996); M. Cvetič and P. Langacker, Mod. Phys. Lett. A **11**, 1247 (1996).
 - [5] J. L. Hewett and T. G. Rizzo, Phys. Rept. **183**, 193 (1989).
 - [6] C. T. Hill and E. H. Simmons, Phys. Rept. **381**, 235 (2003).
 - [7] J. E. Kim and H. P. Nilles, Phys. Lett. B **138**, 150 (1984); D. Suematsu and Y. Yamagishi, Int. J. Mod. Phys. A **10**, 4521 (1995); M. Cvetič and P. Langacker, Mod. Phys. Lett. A **11**, 1247 (1996); V. Jain and R. Shrock, arXiv:hep-ph/9507238; D. A. Demir, Phys. Rev. D **59**, 015002 (1999); H. S. Lee, K. T. Matchev and T. T. Wang, Phys. Rev. D **77**, 015016 (2008).
 - [8] P. Minkowski, Phys. Lett. B **67**, 421 (1977); R. N. Mohapatra and G. Senjanovic, Phys. Rev. Lett. **44**, 912 (1980).
 - [9] J. h. Kang, P. Langacker and T. j. Li, Phys. Rev. D **71**, 015012 (2005).
 - [10] D. A. Demir, L. L. Everett and P. Langacker, Phys. Rev. Lett. **100**, 091804 (2008).
 - [11] D. A. Demir and Y. Farzan, JHEP **0603**, 010 (2006).
 - [12] S. Heinemeyer, O. Stal and G. Weiglein, Phys. Lett. B **710**, 201 (2012).
 - [13] G. G. Ross, K. Schmidt-Hoberg and F. Staub, JHEP **1208**, 074 (2012) [arXiv:1205.1509 [hep-ph]].
 - [14] A. Ali, D. A. Demir, M. Frank and I. Turan, Phys. Rev. **D79**, 095001 (2009).
 - [15] J. Erler, P. Langacker and T. j. Li, Phys. Rev. D **66**, 015002 (2002).
 - [16] C. W. Chiang and E. Senaha, JHEP **0806**, 019 (2008).
 - [17] D. A. Demir, M. Frank, L. Selbuz and I. Turan, Phys. Rev. D **83**, 095001 (2011).
 - [18] M. Frank, L. Selbuz, L. Solmaz and I. Turan, *in preparation*.
 - [19] G. Aad *et al.* [ATLAS Collaboration], Eur. Phys. J. **C 72**, 2174 (2012); G. Aad *et al.* [ATLAS Collaboration], Phys. Lett. **B 715**, 44 (2012); G. Aad *et al.* [ATLAS Collaboration], Phys. Rev. Lett. **108**, 181802 (2012); [S. Chatrchyan *et al.* [CMS Collaboration], Phys. Rev. **D85**, 012004 (2012).

- [20] K. Schmidt-Hoberg and F. Staub, [arXiv:1208.1683 [hep-ph]]; H. An, T. Liu and L. -T. Wang, [arXiv:1207.2473 [hep-ph]], A. Delgado, G. Nardini and M. Quiros, [arXiv:1207.6596 [hep-ph]]; L. Basso and F. Staub, [arXiv:1210.7946 [hep-ph]].
- [21] G. Aad *et al.* [ATLAS Collaboration], arXiv:1208.2884 [hep-ex]. G. Aad *et al.* [ATLAS Collaboration], arXiv:1208.3144 [hep-ex]. [The ATLAS Collaboration, ATLAS-2012-CONF-2012-041, 2012; G. Aad *et al.* [ATLAS Collaboration], [arXiv:1204.5638 [hep-ex]].
- [22] S. Chatrchyan *et al.* [CMS Collaboration], arXiv:1209.6620 [hep-ex]. S. Chatrchyan *et al.* [CMS Collaboration], JHEP **1206**, 169 (2012); S. Chatrchyan *et al.* [CMS Collaboration], Phys. Lett. **B 704**, 411 (2011).
- [23] H. Baer, C. -h. Chen, F. Paige and X. Tata, Phys. Rev. D **50**, 4508 (1994).
- [24] D. A. Demir, L. L. Everett, M. Frank, L. Selbuz and I. Turan, Phys. Rev. **D81**, 035019 (2010).
- [25] E. Komatsu *et al.* [WMAP Collaboration], [arXiv:1001.4538 [astro-ph.CO]].
- [26] S. Y. Choi, H. E. Harber, J. Jalinowski and P. M. Zewas, Nicl. Phys. B **778**, 85 (2007).
- [27] M. Battaglia, A. De Roeck, J. R. Ellis, F. Gianotti, K. A. Olive and L. Pape, Eur. Phys. J. C **33**, 273 (2004); M. Battaglia, A. De Roeck, J. R. Ellis *et al.*, Eur. Phys. J. **C22**, 535-561 (2001).
- [28] See the URL: <http://theory.sinp.msu.ru/~pukhov/calchep.html>; A. Pukhov, [arXiv:hep-ph/0412191].
- [29] A. Semenov, [arXiv:0805.0555 [hep-ph]]; A. Semenov, Comput. Phys. Commun. **115**, 124 (1998).
- [30] M. R. Whalley, D. Bourilkov, R. C. Group, [arXiv: hep-ph/0508110].
- [31] G. Belanger, F. Boudjema, A. Pukhov *et al.*, Comput. Phys. Commun. **180**, 747-767 (2009); G. Belanger, F. Boudjema, P. Brun *et al.*, [arXiv:1004.1092 [hep-ph]].
- [32] D. N. Spergel *et al.* [WMAP Collaboration], Astrophys. J. Suppl. **170**, 377 (2007).
- [33] <http://physics.ucdavis.edu/~conway/research/software/pgs/pgs4-general.htm>.